

Cite as: Y. Pertot *et al.*, *Science*  
10.1126/science.aah6114 (2017).

# Time-resolved x-ray absorption spectroscopy with a water window high-harmonic source

Yoann Pertot,<sup>1</sup> Cédric Schmidt,<sup>2</sup> Mary Matthews,<sup>1,2</sup> Adrien Chauvet,<sup>2\*</sup> Martin Huppert,<sup>1</sup> Vit Svoboda,<sup>1</sup> Aaron von Conta,<sup>1</sup> Andres Tehlar,<sup>1</sup> Denitsa Baykusheva,<sup>1</sup> Jean-Pierre Wolf,<sup>2</sup> Hans Jakob Wörner<sup>1†</sup>

<sup>1</sup>Laboratorium für Physikalische Chemie, ETH Zürich, 8092 Zürich, Switzerland. <sup>2</sup>GAP-Biophotonics, Université de Genève, 1205 Geneva, Switzerland.

\*Present address: Department of Chemistry, University of Sheffield, Sheffield S10 2TN, UK.

†Corresponding author. Email: hwoerner@ethz.ch

Time-resolved X-ray absorption spectroscopy (TR-XAS) has so far practically been limited to large-scale facilities, to sub-picosecond temporal resolution and to the condensed phase. Here, we report the realization of TR-XAS with a temporal resolution in the low femtosecond range by developing a table-top high-harmonic source reaching up to 350 eV, thus partially covering the spectral region of 280 to 530 eV, where water is transmissive. We use this source to follow previously unexamined light-induced chemical reactions in the lowest electronic states of isolated  $\text{CF}_4^+$  and  $\text{SF}_6^+$  molecules in the gas phase. By probing element-specific core-to-valence transitions at the carbon K-edge or the sulfur L-edges, we characterize their reaction paths and observe the effect of symmetry breaking through the splitting of absorption bands and Rydberg-valence mixing induced by the geometry changes.

The application of X-ray sources to the study of the structure of matter has led to some of the most prominent advances in science in the 20th century, be it by diffraction (1) or spectroscopy (2). In the 21st century, the temporal dimension has been added to X-ray measurements, both at synchrotrons (3) and through the recent development of free-electron lasers (4–7). In parallel to these efforts, incoherent tabletop hard X-ray sources have been applied to picosecond time-resolved studies (8, 9). An alternative approach to generating soft X-rays with the advantages of full temporal and spatial coherence, as well as perfect temporal synchronization, is provided by high-harmonic generation. Very early efforts were successful at generating a modest soft-X-ray flux from titanium:sapphire drivers (10–12). Considerable progress came through the extension to longer-wavelength drivers (13–18). However, time-resolved measurements with such sources have so far remained out of reach.

Here, we describe a femtosecond time-resolved experiment using soft-X-ray supercontinua reaching into the water window. Using a long-wavelength driver (1.8  $\mu\text{m}$ ) with exceptional average power (2.5 W, i.e., 2.5 mJ at 1 kHz), we generate soft-X-ray supercontinua ranging from 100 to 350 eV, thus covering the chemically and biologically important K-edge of carbon. We use this source to study dissociation reactions of molecular cations, that have previously not been resolved in time, by transient absorption at the K-edge of carbon and all L-edges of sulfur simultaneously. This development considerably extends pioneering work on transi-

ent absorption in the extreme ultraviolet (19–22). These studies were limited to photon energies below 100 eV, and therefore to the L-edge of silicon and the M- and N-edges of heavier elements.

Our measurements probe the spatial structure of unoccupied orbitals and associated changes along the photochemical reaction pathways. Exploiting the sensitivity of X-ray absorption near-edge structure (XANES) spectroscopy to chemical shifts, we follow the evolution of the unoccupied valence orbitals of molecules from the neutral to the cation and along the reaction path to the final products. Using the sensitivity of dipole selection rules to molecular symmetry, we observe a splitting of some of the initially triply-degenerate orbitals of  $\text{CF}_4$  and  $\text{SF}_6$  to doubly- or nondegenerate orbitals as a consequence of the symmetry lowering induced by photodissociation.

In the experiment we focus a mid-infrared (MIR) femtosecond pulse centered at 1.8  $\mu\text{m}$  into a differentially-pumped high-pressure neon gas cell (Fig. 1A). A toroidal mirror images the soft X-ray (SXR) generation region into a target-gas cell where it is superimposed with a near-infrared (NIR) pulse centered at 800 nm. The SXR absorption of  $\text{CF}_4$  (Fig. 1B) is dominated by overlapping transitions from the carbon 1s shell to the  $5t_2$  and  $6t_2$  unoccupied orbitals of dominant  $\sigma^*$  character that peak at 298 eV. These assignments are based on our time-dependent density-functional theory (TDDFT) calculations of core-shell absorption spectra that use the LB94 functional and the QZ4P basis set (valence quadruple zeta + 4 polarization functions, relativisti-

cally optimized) and are consistent with high-resolution spectra recorded at synchrotron facilities (23). The SXR absorption spectrum of SF<sub>6</sub> (Fig. 1C) is dominated by transitions from the sulfur 2p<sub>1/2</sub> and 2p<sub>3/2</sub> shells to the a<sub>1g</sub> unoccupied orbital and to the shape resonances of t<sub>2g</sub> and e<sub>g</sub> symmetry lying above the L<sub>2,3</sub>-edge. A weaker absorption feature at 240 eV is assigned to the transition from the sulfur 2s shell to the anti-bonding orbital of t<sub>1u</sub> symmetry, lying just below the L<sub>1</sub> edge, which is also consistent with the synchrotron literature (24). The weak modulation observed in both spectra up to energies of 180 eV corresponds to harmonic structure. The experimentally determined resolution of  $E/\Delta E = 308$  suggests that the appearance of these spectra is not spectrometer limited.

Strong-field ionization of neutral CF<sub>4</sub> in the gas phase is induced by an ultrashort NIR pulse centered at 800 nm, focused to a peak intensity of  $(4-5) \times 10^{14}$  W/cm<sup>2</sup>. Ionization of CF<sub>4</sub> to each of the three lowest-lying electronic states of CF<sub>4</sub><sup>+</sup>, of respective vertical ionization energies 16.29, 17.51 and 18.54 eV (measured from the neutral ground state) (25), results in spontaneous dissociation into CF<sub>3</sub><sup>+</sup> and F (26). At positive delays, an increase of the absorbance and a red shift of its maximum are observed in the TR-XAS spectra (Fig. 2B). After reaching a maximal absorbance, the absorption spectrum progressively splits into multiple bands, as illustrated by the sample spectrum (averaged over delays of 300 to 500 fs) shown as inset in Fig. 2B. Most prominently, one band is observed to shift to lower photon energies by 10 eV, terminating at 288 eV. Two further bands shift up and down by 1 eV, respectively, and a fourth band appears as a shoulder of the absorption spectrum around 302 eV. A 50% fraction of the static CF<sub>4</sub> absorption spectrum has been subtracted from the whole data set (Fig. 2B) to account for partial ionization of the probed sample. This fraction has been obtained by comparing the absorption spectrum at long delays with calculated spectra of CF<sub>3</sub><sup>+</sup>. The delay in the appearance of the isolated absorption band of CF<sub>3</sub><sup>+</sup> has been determined by integrating the signal at each delay over a narrow energy range and fitting an error function to the time-dependent signal. This analysis reveals a time delay of  $(40 \pm 2)$  fs in the appearance of the absorption band and provides a time resolution of  $(40 \pm 5)$  fs (see text S2).

The observed changes in the absorption spectrum are the signature of symmetry lowering that occurs when the initially tetrahedral CF<sub>4</sub><sup>+</sup> molecule dissociates into the trigonal planar CF<sub>3</sub><sup>+</sup> molecule. Descent-in-symmetry arguments from group theory combined with dipole-selection rules show that a transition of the type C 1s → t<sub>2</sub> in CF<sub>4</sub> must split into two transitions of the type C 1s → a<sub>2'</sub> and C 1s → e' in CF<sub>3</sub><sup>+</sup>, as observed in Fig. 2B and illustrated in Fig. 2C.

Further insight is obtained by comparison with advanced quantum-chemical *ab-initio* calculations (stick spec-

trum in Fig. 2B and Fig. 3), which are further described in text S3. The X-ray absorption spectrum of CF<sub>4</sub> is dominated by transitions to the 5t<sub>2</sub> and 6t<sub>2</sub> orbitals, which appear as two intense lines at the bottom of Fig. 3A. Along the reaction path, the transition to the 5t<sub>2</sub> orbital first splits into transitions to three nondegenerate orbitals in CF<sub>4</sub><sup>+</sup>. This is the signature of the Jahn-Teller effect which causes the minimum-energy geometry to be of C<sub>2v</sub> symmetry for short ( $\leq 1.6$  Å) C-F bond lengths (27). With increasing bond length, the minimum-energy geometry changes to D<sub>3h</sub>, which is accompanied by the merging of the second- and third-lowest transitions to a single line corresponding to a transition to the 5e' orbital, which confirms the symmetry arguments given in the preceding paragraph.

Figure 3A also reveals a very large shift of the lowest-energy X-ray-absorption band occurring in the transition from CF<sub>4</sub><sup>+</sup> to CF<sub>3</sub><sup>+</sup>. The major part of this shift originates from the changing energy of the unoccupied 2a<sub>2'</sub> orbital, caused by its evolution along the reaction path as shown in Fig. 3B. We next consider the complementarity of the intensity evolutions in the 5e' and 6e' transitions. In the tetrahedral geometry of CF<sub>4</sub>, the 5t<sub>2</sub> orbital has dominant valence character, whereas the 6t<sub>2</sub> orbital has dominant Rydberg character with most of its probability located outside the sphere defined by the fluorine atoms. This arises because the high electron density at the strongly electronegative fluorine atoms creates an effective potential barrier along the radial direction. This so-called "cage effect" has first been discussed in the context of XANES spectra of SF<sub>6</sub> to which we return below (28). As the CF<sub>4</sub><sup>+</sup> molecule dissociates, the fluorine cage opens up, going from a tetrahedral geometry to a planar one in CF<sub>3</sub><sup>+</sup>. This evolution causes a mixing of Rydberg and valence character of the orbitals. Indeed, orbitals previously localized inside (valence) or outside (Rydberg) the cage display a mixed character after dissociation. This change causes a decrease of the overlap between the highly localized core orbital and the initially localized valence orbitals, translating into a decrease of their absorption as the cage opens. In contrast, Rydberg orbitals with initially small overlap with the core orbital exhibit an increase of their absorption as the cage opens up. Along the dissociation coordinate the 5e' orbital therefore develops partial Rydberg character, whereas the 6e' orbital acquires partial valence character (see Fig. 3B). This explains both the calculated and the observed intensity variations, i.e., a decreasing intensity for the transition leading to the 5e' orbital and an increase of the transition strength to the 6e' orbital. The appearance of the shoulder on the high-energy side of the absorption spectrum around 302 eV (Fig. 2B) is also reproduced by the calculations shown in Fig. 3A and is attributed to the 7t<sub>2</sub> orbital acquiring partial valence character as it

evolves into the  $7e'$  orbital of  $CF_3^+$ .

The good agreement between experimental and theoretical results enabled us to reconstruct the average C-F internuclear separation as a function of time during the dissociation of  $CF_4^+$ . These results are shown in text S4 and fig. S10. Moreover, the analysis of time-dependent energy shifts of the  $2a_{2'}$  absorption band provides evidence for the transient excitation of vibrational modes during the dissociation process (text S4 and fig. S11).

We proceeded to demonstrate the generality of our technique by turning to the sulfur L-edges and studying the photodissociation  $SF_6^+ \rightarrow SF_5^+ + F$ . The three lowest electronic states of  $SF_6^+$  of respective vertical ionization energies 15.7, 17.0 and 17.0 eV (measured as energy difference from the neutral ground state) (29), all dissociate to  $SF_5^+ + F$  (26).

Figure 4, C and D, show the observed time-resolved XANES spectra following strong-field ionization of  $SF_6$ , observed at the  $L_{2,3}$ -edge and the  $L_1$ -edge of sulfur simultaneously. A 55% fraction of the static  $SF_6$  absorption spectrum has been subtracted from the whole data sets (Fig. 4, C and D) for clarity, for the same reason as in Fig. 2B. The  $L_{2,3}$ -XANES spectrum at negative delays is dominated by transitions from the sulfur 2p shell of  $SF_6$  to the unoccupied orbital of  $a_{1g}$  symmetry, lying below the  $L_{2,3}$  edge, and to the shape resonances of  $t_{2g}$  and  $e_g$  symmetry lying above (see Fig. 4B). These shape resonances are confined by the effective potential barrier created by the presence of the surrounding electronegative fluorine atoms (28), as we have discussed in the case of  $CF_4$ . However, in  $SF_6$ , they are contained within the cage and therefore have considerable overlap with the central sulfur atom, which explains their strength in the experimental absorption spectra. The  $a_{1g}$  band shifts to lower energies by 2 eV, the  $t_{2g}$  band splits into two main components that shift to lower energies by 2.5 and 6.5 eV, respectively, and the  $e_g$  band shifts to lower energies and broadens considerably. The red shift of all of these absorption bands is consistent with an increase of the local electron density on the sulfur atom, which is a consequence of the loss of an electron-withdrawing fluorine atom. The delay in the appearance of the absorption bands of  $SF_5^+$  has been determined by integrating the signal at each delay over a narrow energy range and fitting an error function to the time-dependent signal. This analysis reveals time delays ranging from  $(34 \pm 4)$  fs to  $(74 \pm 10)$  fs in the appearance of the absorption bands and provides a time resolution of  $(45 \pm 7)$  fs (table S1 and text S2). The absorption at the  $L_1$ -edge (Fig. 4D) is dominated by the transition to a  $t_{1u}$  antibonding orbital, which is observable because of the *gerade* parity of the 2s initial orbital. This band splits into two main components that shift to lower energies by 6 and 15 eV, respectively.

The changes observed in the TR-XAS spectra of  $SF_6$  can

again be assigned by group theory.  $SF_6^+$  in each of its lowest three electronic states can only dissociate into  $SF_5^+$  in its electronic ground state, which has a trigonal bipyramidal geometry and belongs to the  $D_{3h}$  point group. By symmetry, the transition to the  $a_{1g}$  orbital of  $SF_6$  should correlate with a transition leading to an  $a_{1'}$  orbital in the  $D_{3h}$  point group of  $SF_5^+$ . Similarly, the  $t_{2g}$  shape resonance of  $SF_6$  will correlate with  $a_{1'}$  and  $e'$  or  $e''$  shape resonances in  $SF_5^+$ . Finally, the  $e_g$ -symmetry shape resonance should correlate with an  $e'$ - or  $e''$ -symmetric resonance in  $SF_5^+$ . These symmetry correlations precisely describe the experimental observations. The absorption bands corresponding to the unoccupied  $a_{1g}$  orbital and the  $e_g$  shape resonance are both observed to shift to lower energies, without apparent sign of splitting. In contrast, the absorption band corresponding to the  $t_{2g}$  shape resonance is observed to split into two bands. Whereas the shift of all transitions happens almost simultaneously (figs. S12 and S13), the splitting of the  $t_{2g}$  band is delayed by 70 fs. Calculations (text S5) suggest that this delayed splitting is caused by a higher sensitivity of the valence-type orbital characteristic of the  $t_{2g}$  shape resonance in  $SF_6$  to bond angle changes, as compared to the  $a_{1g}$  and  $e_g$  orbitals (fig. S16). The observed splitting of the absorption band would then be driven by rapid changes in bond angles of the  $SF_5^+$  unit that occur around values of 2.5-3 Å for the  $SF_5^+$ -F dissociation coordinate.

Qualitatively similar dynamics are observed at the  $L_1$  edge. By symmetry, the dominant  $2s \rightarrow t_{1u}$  transition can only split into two transitions leading to orbitals of  $e'$  or  $a_{2'}$  symmetries, which corresponds well to the experimental observation of a splitting into two bands. The broad absorption feature observed around 267 eV corresponds to several absorption bands, all located above the  $L_1$  edge (244.17 eV). These bands correspond to shape resonances which have a very short lifetime and, therefore, a large natural linewidth leading to the observation of a single very broad absorption feature.

Our results demonstrate the feasibility of time-resolved XAS with tabletop light sources and its potential in elucidating the dynamics of electrons and nuclei in chemical reactions. Specifically, this method nicely complements other key techniques in molecular reaction dynamics, such as time-resolved photoelectron spectroscopy (30) and time-resolved high-harmonic spectroscopy (31). We therefore anticipate TR-XAS to become a decisive technique for the investigation of nonadiabatic molecular dynamics, such as those occurring at conical intersections (32, 33). Owing to its sensitivity to elements, TR-XAS will enable time-resolved studies of electronic dynamics with atomic spatial sensitivity. Broadening the spectral coverage of our source only slightly would bring time-resolved extended X-ray absorp-

tion fine structure (TR-EXAFS) in combination with X-ray absorption near edge structure (XANES) experiments within reach, providing full structural and electronic information. Although demonstrated in the gas phase, our method is directly applicable to the solid state and is readily extendable to the liquid phase using flow cells (34) or flat microjets (35).

## REFERENCES AND NOTES

- M. H. F. Wilkins, A. R. Stokes, H. R. Wilson, Molecular structure of deoxyribose nucleic acids. *Nature* **171**, 738–740 (1953). [doi:10.1038/171738a0](https://doi.org/10.1038/171738a0) [Medline](#)
- J. A. van Bokhoven, C. Lamberti, Eds., *X-Ray Absorption and X-Ray Emission Spectroscopy: Theory and Applications* (Wiley, 2016).
- Ch. Bressler, C. Milne, V.-T. Pham, A. Elnahas, R. M. van der Veen, W. Gawelda, S. Johnson, P. Beaud, D. Grolimund, M. Kaiser, C. N. Borca, G. Ingold, R. Abela, M. Chergui, Femtosecond XANES study of the light-induced spin crossover dynamics in an iron(II) complex. *Science* **323**, 489–492 (2009). [doi:10.1126/science.1165733](https://doi.org/10.1126/science.1165733) [Medline](#)
- W. Ackermann, G. Asova, V. Ayvazyan, A. Azima, N. Baboi, J. Bähr, V. Balandin, B. Beutner, A. Brandt, A. Bolzmann, R. Brinkmann, O. I. Brovko, M. Castellano, P. Castro, L. Catani, E. Chiadroni, S. Choroba, A. Cianchi, J. T. Costello, D. Cubaynes, J. Dardis, W. Decking, H. Delsim-Hashemi, A. Delsérieys, G. Di Pirro, M. Dohlus, S. Düsterer, A. Eckhardt, H. T. Edwards, B. Faatz, J. Feldhaus, K. Flöttmann, J. Frisch, L. Fröhlich, T. Garvey, U. Gensch, C. Gerth, M. Görler, N. Golubeva, H.-J. Grabosch, M. Grecki, O. Grimm, K. Hacker, U. Hahn, J. H. Han, K. Honkavaara, T. Hott, M. Hüning, Y. Ivanisenko, E. Jaeschke, W. Jalmuzna, T. Jezynski, R. Kammering, V. Katalev, K. Kavanagh, E. T. Kennedy, S. Khodyachykh, K. Klose, V. Kocharyan, M. Körfer, M. Kollwe, W. Koprek, S. Korepanov, D. Kostin, M. Krassilnikov, G. Kube, M. Kuhlmann, C. L. S. Lewis, L. Lilje, T. Limberg, D. Lipka, F. Löh, H. Luna, M. Luong, M. Martins, M. Meyer, P. Michelato, V. Mitchev, W. D. Möller, L. Monaco, W. F. O. Müller, O. Napieralski, O. Napoly, P. Nicolosi, D. Nölle, T. Nuñez, A. Oppelt, C. Pagani, R. Paparella, N. Pchalek, J. Pedregosa-Gutierrez, B. Petersen, B. Petrosyan, G. Petrosyan, L. Petrosyan, J. Pflüger, E. Plönjes, L. Poletto, K. Pozniak, E. Prat, D. Proch, P. Pucyk, P. Radcliffe, H. Redlin, K. Rehlich, M. Richter, M. Roehrs, J. Roensch, R. Romaniuk, M. Ross, J. Rossbach, V. Rybnikov, M. Sachwitz, E. L. Saldin, W. Sandner, H. Schlarb, B. Schmidt, P. Schmitz, P. Schmüser, J. R. Schneider, E. A. Schneidmiller, S. Schnepf, S. Schreiber, M. Seidel, D. Sertore, A. V. Shabunov, C. Simon, S. Simrock, E. Sombrowski, A. A. Sorokin, P. Spanknebel, R. Spesyvtsev, L. Staykov, B. Steffen, F. Stephan, F. Stulle, H. Thom, K. Tiedtke, M. Tischer, S. Toleikis, R. Treusch, D. Trines, I. Tsakov, E. Vogel, T. Weiland, H. Weise, M. Wellhöfer, M. Wendt, I. Will, A. Winter, K. Wittenburg, W. Wurth, P. Yeates, M. V. Yurkov, I. Zagorodnov, K. Zapfe, Operation of a free-electron laser from the extreme ultraviolet to the water window. *Nat. Photonics* **1**, 336–342 (2007). [doi:10.1038/nphoton.2007.76](https://doi.org/10.1038/nphoton.2007.76)
- P. Emma, R. Akre, J. Arthur, R. Bionta, C. Bostedt, J. Bozek, A. Brachmann, P. Bucksbaum, R. Coffee, F.-J. Decker, Y. Ding, D. Dowell, S. Edstrom, A. Fisher, J. Frisch, S. Gilevich, J. Hastings, G. Hays, P. Hering, Z. Huang, R. Iverson, H. Loos, M. Messerschmidt, A. Miahnahri, S. Moeller, H.-D. Nuhn, G. Pile, D. Ratner, J. Rzepiela, D. Schultz, T. Smith, P. Stefan, H. Tompkins, J. Turner, J. Welch, W. White, J. Wu, G. Yocky, J. Galayda, First lasing and operation of an ångström-wavelength free-electron laser. *Nat. Photonics* **4**, 641–647 (2010). [doi:10.1038/nphoton.2010.176](https://doi.org/10.1038/nphoton.2010.176)
- T. Ishikawa, H. Aoyagi, T. Asaka, Y. Asano, N. Azumi, T. Bizen, H. Ego, K. Fukami, T. Fukui, Y. Furukawa, S. Goto, H. Hanaki, T. Hara, T. Hasegawa, T. Hatsui, A. Higashiya, T. Hirono, N. Hosoda, M. Ishii, T. Inagaki, Y. Inubushi, T. Itoga, Y. Joti, M. Kago, T. Kameshima, H. Kimura, Y. Kirihara, A. Kiyomichi, T. Kobayashi, C. Kondo, T. Kudo, H. Maesaka, X. M. Maréchal, T. Masuda, S. Matsubara, T. Matsumoto, T. Matsushita, S. Matsui, M. Nagasono, N. Nariyama, H. Ohashi, T. Ohata, T. Ohshima, S. Ono, Y. Otake, C. Saji, T. Sakurai, T. Sato, K. Sawada, T. Seike, K. Shirasawa, T. Sugimoto, S. Suzuki, S. Takahashi, H. Takebe, K. Takeshita, K. Tamasaku, H. Tanaka, R. Tanaka, T. Tanaka, T. Togashi, K. Togawa, A. Tokuhisa, H. Tomizawa, K. Tono, S. Wu, M. Yabashi, M. Yamaga, A. Yamashita, K. Yanagida, C. Zhang, T. Shintake, H. Kitamura, N. Kumagai, A compact X-ray free-electron laser emitting in the sub-ångström region. *Nat. Photonics* **6**, 540–544 (2012). [doi:10.1038/nphoton.2012.141](https://doi.org/10.1038/nphoton.2012.141)
- E. Allaria, R. Appio, L. Badano, W. A. Barletta, S. Bassanese, S. G. Biedron, A. Borgia, E. Busetto, D. Castronovo, P. Cinquegrana, S. Cleva, D. Cocco, M. Cornacchia, P. Craievich, I. Cudin, G. D'Auria, M. Dal Forno, M. B. Danailov, R. De Monte, G. De Ninno, P. Delgiusto, A. Demidovich, S. Di Mitri, B. Diviacco, A. Fabris, R. Fabris, W. Fawley, M. Ferianis, E. Ferrari, S. Ferry, L. Froehlich, P. Furlan, G. Gaio, F. Gelmetti, L. Giannessi, M. Giannini, R. Gobessi, R. Ivanov, E. Karantzoulis, M. Lonza, A. Lutman, B. Mahieu, M. Milloch, S. V. Milton, M. Musardo, I. Nikolov, S. Noe, F. Parmigiani, G. Penco, M. Petronio, L. Pivetta, M. Predonzani, F. Rossi, L. Rumiz, A. Salom, C. Scafuri, C. Serpico, P. Sigalotti, S. Spampinati, C. Spezzani, M. Svandrik, C. Svetina, S. Tazzari, M. Trovo, R. Umer, A. Vascotto, M. Veronese, R. Visintini, M. Zaccaria, D. Zangrando, M. Zangrando, Highly coherent and stable pulses from the FERMI seeded free-electron laser in the extreme ultraviolet. *Nat. Photonics* **6**, 699–704 (2012). [doi:10.1038/nphoton.2012.233](https://doi.org/10.1038/nphoton.2012.233)
- F. Ráksi, K. R. Wilson, Z. Jiang, A. Ikhlef, C. Y. Côté, J.-C. Kieffer, Ultrafast x-ray absorption probing of a chemical reaction. *J. Chem. Phys.* **104**, 6066 (1996). [doi:10.1063/1.471305](https://doi.org/10.1063/1.471305)
- M. Bargheer, N. Zhavoronkov, Y. Gritsai, J. C. Woo, D. S. Kim, M. Woerner, T. Elsaesser, Coherent atomic motions in a nanostructure studied by femtosecond X-ray diffraction. *Science* **306**, 1771–1773 (2004). [doi:10.1126/science.1104739](https://doi.org/10.1126/science.1104739) [Medline](#)
- Ch. Spielmann, N. H. Burnett, S. Sartania, R. Koppitsch, M. Schnürer, C. Kan, M. Lenzner, P. Wobrauschek, F. Krausz, Generation of coherent X-rays in the water window using 5-femtosecond laser pulses. *Science* **278**, 661–664 (1997). [doi:10.1126/science.278.5338.661](https://doi.org/10.1126/science.278.5338.661)
- E. Seres, J. Seres, F. Krausz, C. Spielmann, Generation of coherent soft-X-ray radiation extending far beyond the titanium L edge. *Phys. Rev. Lett.* **92**, 163002 (2004). [doi:10.1103/PhysRevLett.92.163002](https://doi.org/10.1103/PhysRevLett.92.163002) [Medline](#)
- E. Seres, C. Spielmann, Ultrafast soft x-ray absorption spectroscopy with sub-20-fs resolution. *Appl. Phys. Lett.* **91**, 121919 (2007). [doi:10.1063/1.2789732](https://doi.org/10.1063/1.2789732)
- E. J. Takahashi, T. Kanai, K. L. Ishikawa, Y. Nabekawa, K. Midorikawa, Coherent water window x ray by phase-matched high-order harmonic generation in neutral media. *Phys. Rev. Lett.* **101**, 253901 (2008). [doi:10.1103/PhysRevLett.101.253901](https://doi.org/10.1103/PhysRevLett.101.253901) [Medline](#)
- M.-C. Chen, P. Arpin, T. Popmintchev, M. Gerrity, B. Zhang, M. Seaberg, D. Popmintchev, M. M. Murnane, H. C. Kapteyn, Bright, coherent, ultrafast soft X-ray harmonics spanning the water window from a tabletop light source. *Phys. Rev. Lett.* **105**, 173901 (2010). [doi:10.1103/PhysRevLett.105.173901](https://doi.org/10.1103/PhysRevLett.105.173901) [Medline](#)
- T. Popmintchev, M.-C. Chen, D. Popmintchev, P. Arpin, S. Brown, S. Alisauskas, G. Andriukaitis, T. Balciunas, O. D. Mücke, A. Pugzlys, A. Baltuska, B. Shim, S. E. Schrauth, A. Gaeta, C. Hernández-García, L. Plaja, A. Becker, A. Jaron-Becker, M. M. Murnane, H. C. Kapteyn, Bright coherent ultrahigh harmonics in the keV x-ray regime from mid-infrared femtosecond lasers. *Science* **336**, 1287–1291 (2012). [doi:10.1126/science.1218497](https://doi.org/10.1126/science.1218497) [Medline](#)
- N. Ishii, K. Kaneshima, K. Kitano, T. Kanai, S. Watanabe, J. Itatani, Carrier-envelope phase-dependent high harmonic generation in the water window using few-cycle infrared pulses. *Nat. Commun.* **5**, 3331 (2014). [Medline](#)
- S. L. Cousin, F. Silva, S. Teichmann, M. Hemmer, B. Buares, J. Biegert, High-flux table-top soft x-ray source driven by sub-2-cycle, CEP stable, 1.85- $\mu\text{m}$  1-kHz pulses for carbon K-edge spectroscopy. *Opt. Lett.* **39**, 5383–5386 (2014). [doi:10.1364/OL.39.005383](https://doi.org/10.1364/OL.39.005383) [Medline](#)
- F. Silva, S. M. Teichmann, S. L. Cousin, M. Hemmer, J. Biegert, Spatiotemporal isolation of attosecond soft X-ray pulses in the water window. *Nat. Commun.* **6**, 6611 (2015). [doi:10.1038/ncomms7611](https://doi.org/10.1038/ncomms7611) [Medline](#)
- Z. H. Loh, M. Khalil, R. E. Correa, R. Santra, C. Buth, S. R. Leone, Quantum state-resolved probing of strong-field-ionized xenon atoms using femtosecond high-order harmonic transient absorption spectroscopy. *Phys. Rev. Lett.* **98**, 143601 (2007). [doi:10.1103/PhysRevLett.98.143601](https://doi.org/10.1103/PhysRevLett.98.143601) [Medline](#)
- E. Goulielmakis, Z.-H. Loh, A. Wirth, R. Santra, N. Rohringer, V. S. Yakovlev, S. Zherebtsov, T. Pfeifer, A. M. Azzeer, M. F. Kling, S. R. Leone, F. Krausz, Real-time observation of valence electron motion. *Nature* **466**, 739–743 (2010). [doi:10.1038/nature09212](https://doi.org/10.1038/nature09212) [Medline](#)

21. M. Schultze, K. Ramasesha, C. D. Pemmaraju, S. A. Sato, D. Whitmore, A. Gandman, J. S. Prell, L. J. Borja, D. Prendergast, K. Yabana, D. M. Neumark, S. R. Leone, Attosecond band-gap dynamics in silicon. *Science* **346**, 1348–1352 (2014). [doi:10.1126/science.1260311](https://doi.org/10.1126/science.1260311) [Medline](#)
22. A. R. Attar, A. Bhattacharjee, S. R. Leone, Direct observation of the transition-state region in the photodissociation of CH<sub>3</sub>I by femtosecond extreme ultraviolet transient absorption spectroscopy. *J. Phys. Chem. Lett.* **6**, 5072–5077 (2015). [doi:10.1021/acs.jpclett.5b02489](https://doi.org/10.1021/acs.jpclett.5b02489) [Medline](#)
23. K. Ueda, Y. Shimizu, H. Chiba, M. Okunishi, K. Ohmori, Y. Sato, E. Shigemasa, N. Kosugi, C 1s and F 1s photoabsorption and subsequent electronic decay of CH<sub>4</sub>, CH<sub>3</sub>F, CH<sub>2</sub>F<sub>2</sub>, CHF<sub>3</sub>, and CF<sub>4</sub>. *J. Electron Spectrosc. Relat. Phenom.* **79**, 441–444 (1996). [doi:10.1016/0368-2048\(96\)02890-3](https://doi.org/10.1016/0368-2048(96)02890-3)
24. E. Hudson, D. A. Shirley, M. Domke, G. Remmers, A. Puschmann, T. Mandel, C. Xue, G. Kaindl, High-resolution measurements of near-edge resonances in the core-level photoionization spectra of SF<sub>6</sub>. *Phys. Rev. A* **47**, 361–373 (1993). [doi:10.1103/PhysRevA.47.361](https://doi.org/10.1103/PhysRevA.47.361) [Medline](#)
25. D. M. P. Holland, A. W. Potts, A. B. Trofimov, J. Breidbach, J. Schirmer, R. Feifel, T. Richter, K. Godehusen, M. Martins, A. Tutay, M. Yalcinkaya, M. Al-Hada, S. Eriksson, L. Karlsson, An experimental and theoretical study of the valence shell photoelectron spectrum of tetrafluoromethane. *Chem. Phys.* **308**, 43–57 (2005). [doi:10.1016/j.chemphys.2004.07.042](https://doi.org/10.1016/j.chemphys.2004.07.042)
26. J. Creasey, H. M. Jones, D. M. Smith, R. P. Tuckett, P. A. Hatherly, K. Codling, I. Powis, Fragmentation of valence electronic states of CF<sub>4</sub><sup>+</sup> and SF<sub>6</sub><sup>+</sup> studied by threshold photoelectron-photoion coincidence spectroscopy. *Chem. Phys.* **174**, 441–452 (1993). [doi:10.1016/0301-0104\(93\)80010-7](https://doi.org/10.1016/0301-0104(93)80010-7)
27. J. M. Garca de la Vega, E. San Fabián, Jahn-Teller effect and dissociation from the ground state of CF<sub>4</sub><sup>+</sup>. *Chem. Phys.* **151**, 335–342 (1991). [doi:10.1016/0301-0104\(91\)80019-F](https://doi.org/10.1016/0301-0104(91)80019-F)
28. J. L. Dehmer, D. Dill, S. Wallace, Shape-resonance-enhanced nuclear-motion effects in molecular photoionization. *Phys. Rev. Lett.* **43**, 1005–1008 (1979). [doi:10.1103/PhysRevLett.43.1005](https://doi.org/10.1103/PhysRevLett.43.1005)
29. D. M. P. Holland, M. A. MacDonald, P. Baltzer, L. Karlsson, M. Lundqvist, B. Wannberg, W. von Niessen, An experimental and theoretical study of the valence shell photoelectron spectrum of sulphur hexafluoride. *Chem. Phys.* **192**, 333–353 (1995). [doi:10.1016/0301-0104\(94\)00381-J](https://doi.org/10.1016/0301-0104(94)00381-J)
30. T. Suzuki, Femtosecond time-resolved photoelectron imaging. *Annu. Rev. Phys. Chem.* **57**, 555–592 (2006). [doi:10.1146/annurev.physchem.57.032905.104601](https://doi.org/10.1146/annurev.physchem.57.032905.104601) [Medline](#)
31. H. J. Wörner, J. B. Bertrand, D. V. Kartashov, P. B. Corkum, D. M. Villeneuve, Following a chemical reaction using high-harmonic interferometry. *Nature* **466**, 604–607 (2010). [doi:10.1038/nature09185](https://doi.org/10.1038/nature09185) [Medline](#)
32. D. Polli, P. Altoè, O. Weingart, K. M. Spillane, C. Manzoni, D. Brida, G. Tomasello, G. Orlandi, P. Kukura, R. A. Mathies, M. Garavelli, G. Cerullo, Conical intersection dynamics of the primary photoisomerization event in vision. *Nature* **467**, 440–443 (2010). [doi:10.1038/nature09346](https://doi.org/10.1038/nature09346) [Medline](#)
33. H. J. Wörner, J. B. Bertrand, B. Fabre, J. Higuët, H. Ruf, A. Dubrouil, S. Patchkovskii, M. Spanner, Y. Mairesse, V. Blanchet, E. Mével, E. Constant, P. B. Corkum, D. M. Villeneuve, Conical intersection dynamics in NO<sub>2</sub> probed by homodyne high-harmonic spectroscopy. *Science* **334**, 208–212 (2011). [doi:10.1126/science.1208664](https://doi.org/10.1126/science.1208664) [Medline](#)
34. N. Huse, T. K. Kim, L. Jamula, J. K. McCusker, F. M. F. de Groot, R. W. Schoenlein, Photo-induced spin-state conversion in solvated transition metal complexes probed via time-resolved soft X-ray spectroscopy. *J. Am. Chem. Soc.* **132**, 6809–6816 (2010). [doi:10.1021/ja101381a](https://doi.org/10.1021/ja101381a) [Medline](#)
35. M. Ekimova, W. Quevedo, M. Faubel, P. Wernet, E. T. J. Nibbering, A liquid flatjet system for solution phase soft-x-ray spectroscopy. *Struct. Dyn.* **2**, 054301 (2015). [doi:10.1063/1.4928715](https://doi.org/10.1063/1.4928715) [Medline](#)
36. H. Dossmann Soldi-Lose, G. A. Garcia, L. Nahon, B. K. de Miranda, C. Alcaraz, Comprehensive vacuum ultraviolet photoionization study of the CF<sub>3</sub>(●) trifluoromethyl radical using synchrotron radiation. *J. Chem. Phys.* **136**, 204304 (2012). [doi:10.1063/1.4719529](https://doi.org/10.1063/1.4719529) [Medline](#)

## ACKNOWLEDGMENTS

We thank Luigi Bonacina, Andres Laso, Andreas Schneider and Michel Moret for technical support, David Prendergast, Rock Bohinc and Jeroen van Bokhoven for helpful discussions on the calculation of soft-X-ray absorption spectra and Markus Reiher and Christopher Stein for performing supporting calculations. We gratefully acknowledge funding from the NCCR-MUST, a funding instrument of the Swiss National Science Foundation (SNSF), SNSF project no. 200021\_159875, an ERC Starting Grant (Project No. 307270-ATTOSCOPE) and an ERC Advanced Grant (Project No. 291201-FILATMO). Yoann Pertot thanks the ETH Zürich postdoctoral fellowship program for support. Additional data supporting the conclusions are shown in the supplementary material.

## SUPPLEMENTARY MATERIALS

[www.sciencemag.org/cgi/content/full/science.aah6114/DC1](http://www.sciencemag.org/cgi/content/full/science.aah6114/DC1)

Texts S1 to S5

Figs. S1 to S16

Table S1

Reference (36)

21 July 2016; accepted 15 December 2016

Published online 5 January 2017

10.1126/science.aah6114

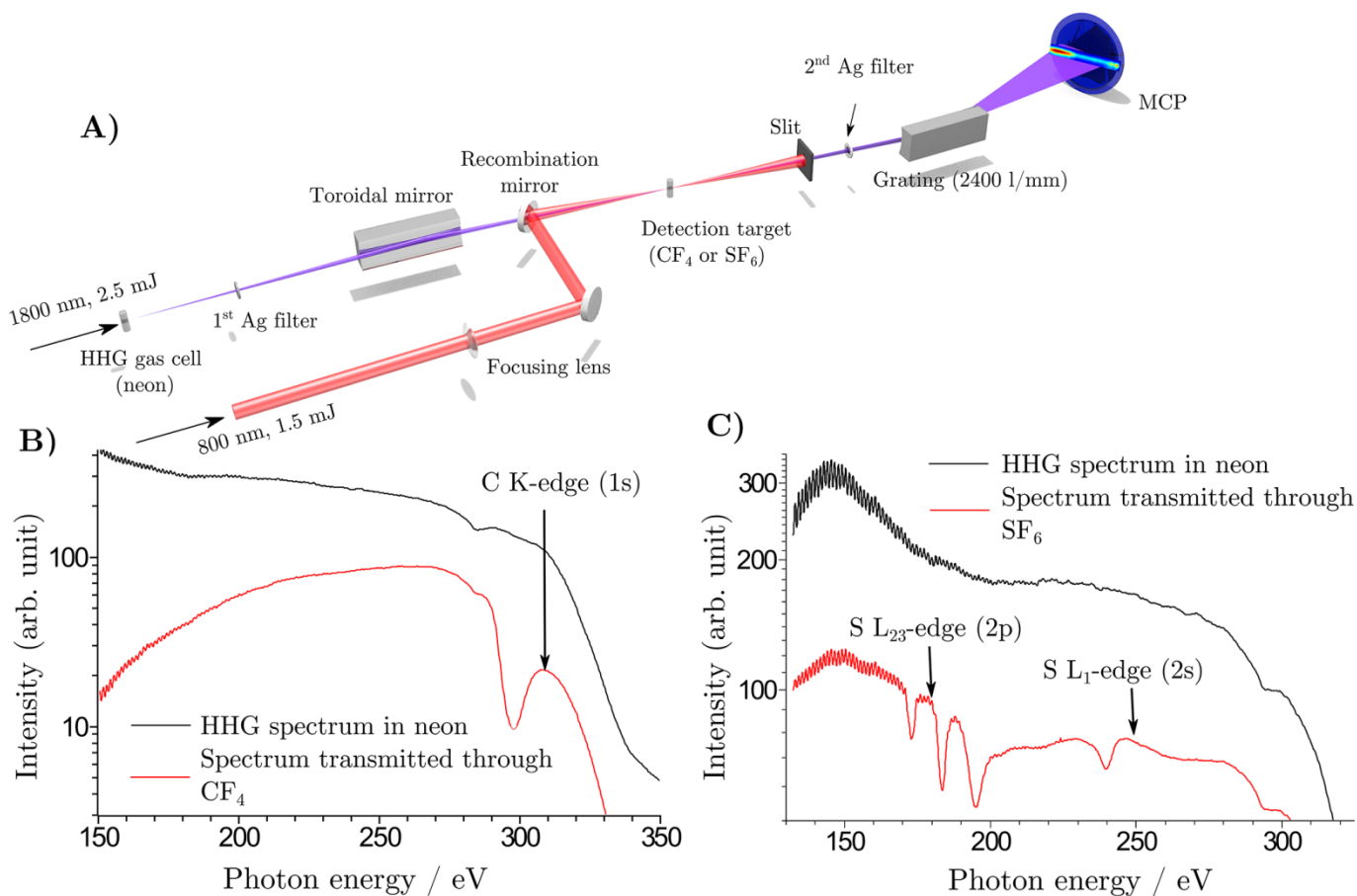


**Fig. 1. Soft-X-ray transient-absorption spectroscopy with a high-harmonic source.** (A) Experimental setup, (B) High-harmonic spectrum at the carbon K-edge and transmitted spectrum through CF<sub>4</sub> gas, (C) High-harmonic spectrum at the sulfur L-edges and transmitted spectrum through SF<sub>6</sub> gas.

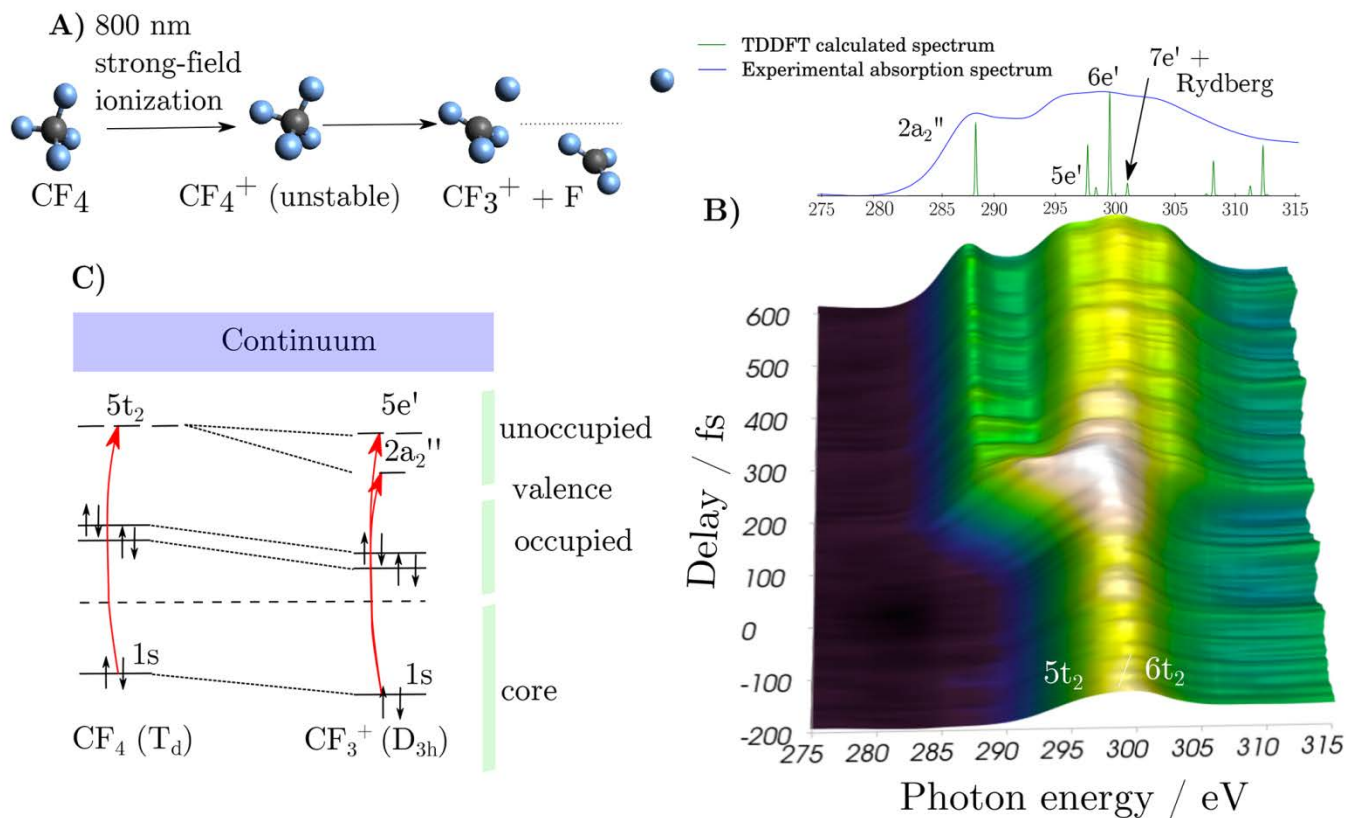


**Fig. 2. Transient-absorption spectroscopy at the carbon K-edge.** (A) An intense near-infrared pulse induces single ionization of  $\text{CF}_4$  to  $\text{CF}_4^+$  which is unstable in its electronic ground state and dissociates into  $\text{CF}_3^+ + \text{F}$ . The sequence of geometries is taken from a calculated minimum-energy reaction path (see text for details). (B) Absorbance  $A(t) = \ln[I_0/I(t)]$  as a function of the SXR-NIR time delay. Negative time delays correspond to the SXR pulse preceding the NIR pulse. The intensity axis, as well as the color scale, are linear. The standard deviation of this data set amounts to 4%. The calculated stick spectrum in the inset has been shifted by -2.5 eV. (C) Orbital diagram illustrating selected transitions, as obtained from TDDFT/LB94 calculations.

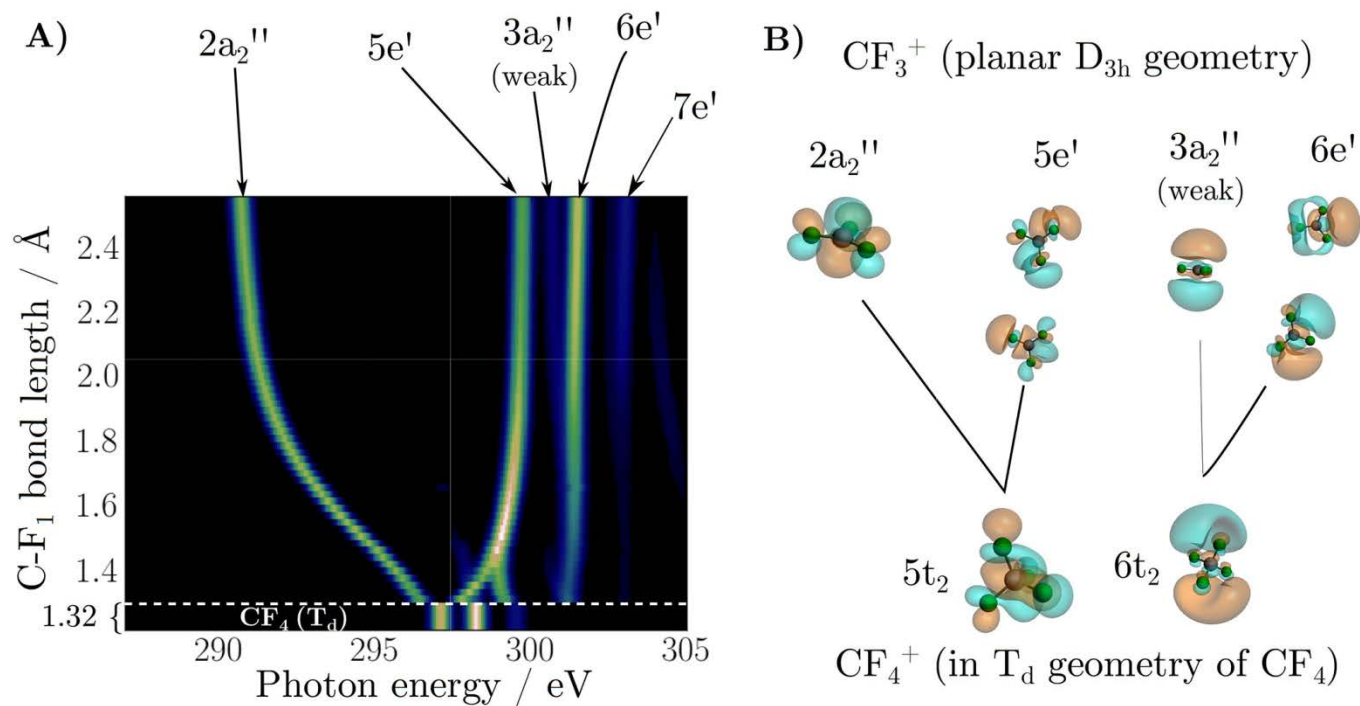


**Fig. 3. Calculated X-ray absorption spectra of the reaction  $\text{CF}_4^+ \rightarrow \text{CF}_3^+ + \text{F}$ .** (A) X-ray absorption spectra, calculated with the TDDFT method using the LB94 functional and the QZ4P basis set, as a function of one C-F internuclear separation along the minimum-energy reaction path  $\text{CF}_4^+ \rightarrow \text{CF}_3^+ + \text{F}$  calculated on the CCSD/6-31G\* level of theory. The  $\text{CF}_4$  X-ray absorption spectrum is shown below the dotted line. A linear intensity scale has been used. (B) Unoccupied orbitals characteristic of the final state of the X-ray transition, corresponding to the dominant absorption bands of (A). Only one of three equivalent orbitals is shown in the tetrahedral ( $T_d$ ) geometry of  $\text{CF}_4^+$ , whereas both, distinct orbitals of  $e'$  symmetry are shown for  $\text{CF}_3^+$ .

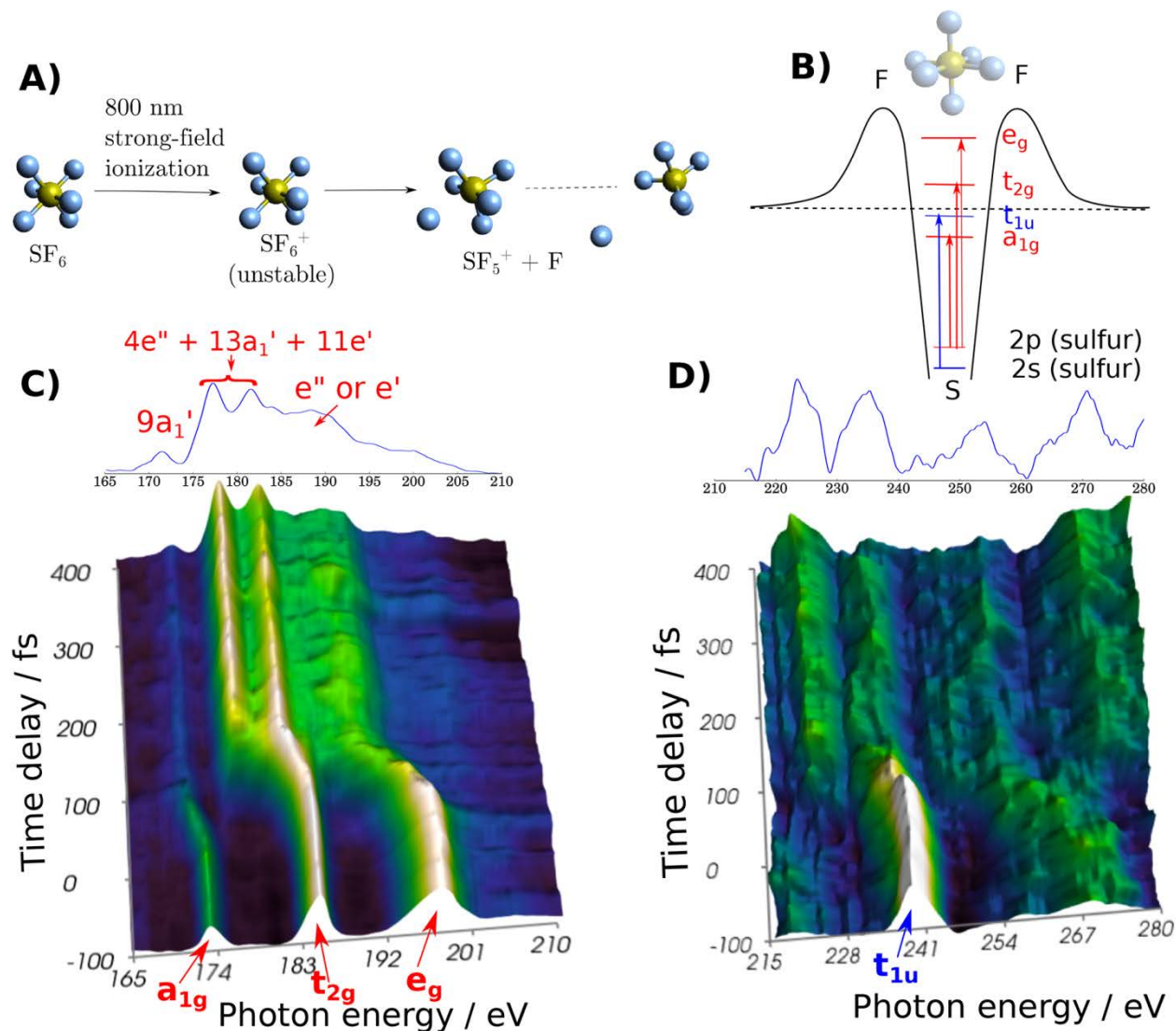


**Fig. 4. Transient absorption spectroscopy at the sulfur L-edges.** (A) An intense infrared pulse induces single ionization of  $\text{SF}_6$  to  $\text{SF}_6^+$  which is unstable in its electronic ground state and dissociates into  $\text{SF}_5^+ + \text{F}$ . The sequence of geometries is taken from a calculated minimum-energy reaction path. (B) Orbital diagram illustrating the experimentally observed transitions. (C) Absorbance  $A(t) = \ln[I_0/I(t)]$  at the  $L_{2,3}$ -edge as a function of the SXR-NIR time delay. Negative time delays correspond to the SXR pulse preceding the NIR pulse. The standard deviation of this data set amounts to 4.3%. (D) Absorbance at the  $L_1$ -edge of  $\text{SF}_6$ . The insets show absorption spectra obtained by averaging over delays of 200 to 400 fs. All intensity axes shown in this figure, as well as all color scales, are linear. The standard deviation of this data set amounts to 6.3%.

EXTENDED PDF FORMAT  
SPONSORED BY



**Time-resolved x-ray absorption spectroscopy with a water window  
high-harmonic source**

Yoann Pertot, Cédric Schmidt, Mary Matthews, Adrien Chauvet, Martin Huppert, Vit Svoboda, Aaron von Conta, Andres Tehlar, Denitsa Baykusheva, Jean-Pierre Wolf and Hans Jakob Wörner (January 5, 2017)

published online January 5, 2017

Editor's Summary

---

This copy is for your personal, non-commercial use only.

---

- Article Tools** Visit the online version of this article to access the personalization and article tools:  
<http://science.sciencemag.org/content/early/2017/01/04/science.aah6114>
- Permissions** Obtain information about reproducing this article:  
<http://www.sciencemag.org/about/permissions.dtl>

*Science* (print ISSN 0036-8075; online ISSN 1095-9203) is published weekly, except the last week in December, by the American Association for the Advancement of Science, 1200 New York Avenue NW, Washington, DC 20005. Copyright 2016 by the American Association for the Advancement of Science; all rights reserved. The title *Science* is a registered trademark of AAAS.